iScience

CellPress
OPEN ACCESS

Article

Lipid flippase dysfunction as a therapeutic target for endosomal anomalies in Alzheimer's disease

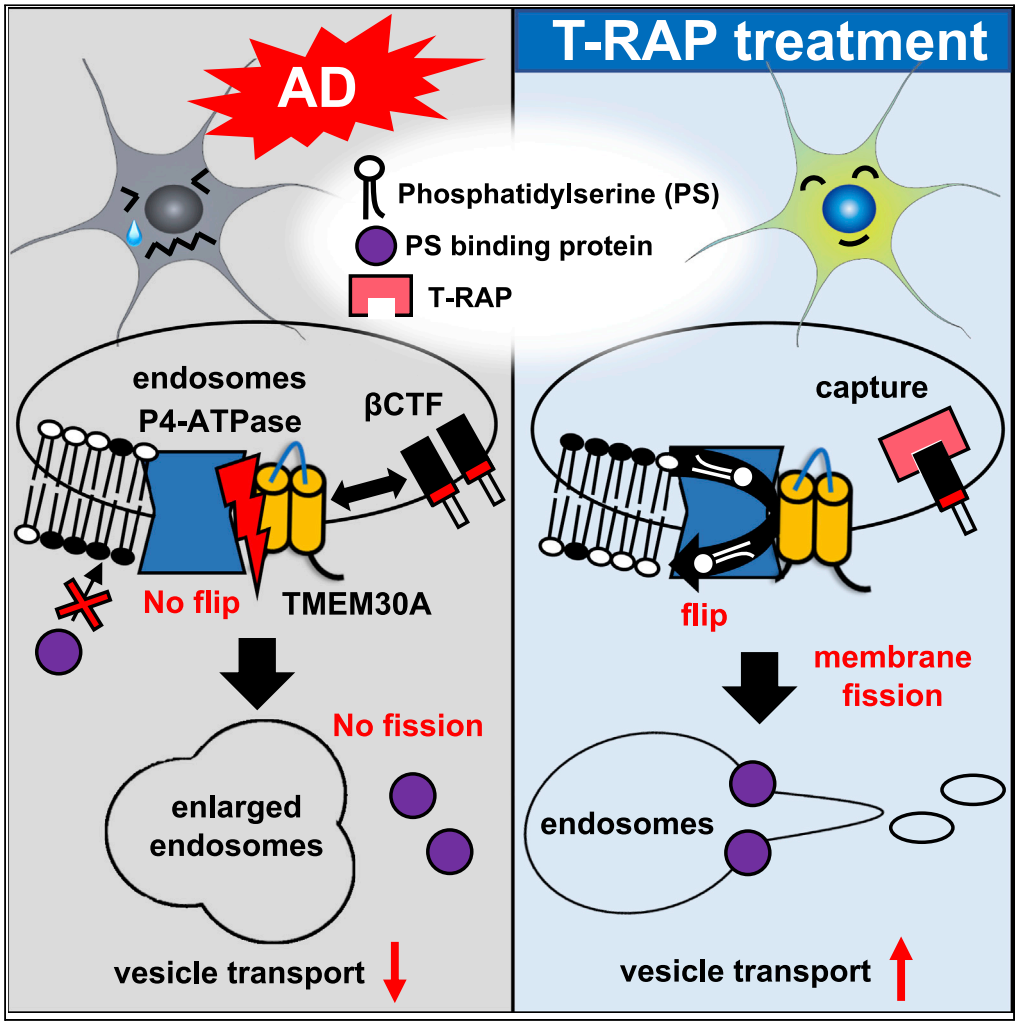

Nanaka Kaneshiro, Masato Komai, Ryosuke Imaoka, ..., Takashi Sakurai, Takashi Uehara, Nobumasa Takasugi

ntakasu@okayama-u.ac.jp

Highlights

Interaction between βCTF and TMEM30A mediates endosomal anomalies

Accumulated βCTF impairs lipid flippase function, a regulator of vesicle transport

Age-dependent lipid flippase disorder can precede Aβ deposition in AD model mice

βCTF interacting peptide, 'T-RAP' can improve βCTF mediated endosomal anomalies

Kaneshiro et al., iScience 25, 103869
March 18, 2022 © 2022 The Author(s).
https://doi.org/10.1016/j.isci.2022.103869

iScience

CellPress
OPEN ACCESS

Article

Lipid flippase dysfunction as a therapeutic target for endosomal anomalies in Alzheimer's disease

Nanaka Kaneshiro,[1,2] Masato Komai,[1] Ryosuke Imaoka,[1] Atsuya Ikeda,[1] Yuji Kamikubo,[3] Takashi Saito,[4,5] Takaomi C. Saido,[5] Taisuke Tomita,[6] Tadafumi Hashimoto,[7] Takeshi Iwatsubo,[7] Takashi Sakurai,[3] Takashi Uehara,[1] and Nobumasa Takasugi[1,3,8,*]

SUMMARY

Endosomal anomalies because of vesicular traffic impairment have been indicated as an early pathology of Alzheimer'| disease (AD). However, the mechanisms and therapeutic targets remain unclear. We previously reported that βCTF, one of the pathogenic metabolites of APP, interacts with TMEM30A. TMEM30A constitutes a lipid flippase with P4-ATPase and regulates vesicular trafficking through the asymmetric distribution of phospholipids. Therefore, the alteration of lipid flippase activity in AD pathology has got attention. Herein, we showed that the interaction between βCTF and TMEM30A suppresses the physiological formation and activity of lipid flippase in AD model cells, A7, and $App^{NL-G-F/NL-G-F}$ model mice. Furthermore, the T-RAP peptide derived from the βCTF binding site of TMEM30A improved endosomal anomalies, which could be a result of the restored lipid flippase activity. Our results provide insights into the mechanisms of vesicular traffic impairment and suggest a therapeutic target for AD.

INTRODUCTION

Amyloid-β (Aβ) peptides are accumulated in the brains of patients with Alzheimer's disease (AD) (Hardy and Selkoe, 2002) and are produced from the sequential cleavage of the β-amyloid precursor protein (APP) by the β-site APP cleaving enzyme 1 (BACE1) (Vassar et al., 1999; Sinha et al., 1999; Yan et al., 1999) and γ-secretase (Takasugi et al., 2003). Although pieces of genetic and biological evidence suggest the link between Aβ and AD pathogenesis, several clinical trials based on the "amyloid hypothesis" have failed (Huang et al., 2020). Therefore, new ideas and therapeutic targets that complement the hypothesis are required for this field.

A previous report identified that traffic impairment, showing endosomal anomalies, is an early pathogenic event in AD before Aβ deposition (Cataldo et al., 2000). In line with this, several studies in AD model mice (Lauritzen et al., 2012), human iPSC-derived neurons (Kwart et al., 2019), and AD brains (Kim et al., 2016) have shown that the accumulated β-carboxyl-terminal fragment of APP (βCTF), the product of BACE1 and direct precursor of Aβ, is the cause of endosomal anomalies. Indeed, BACE1 expression and activity are upregulated at the early stage of sporadic AD (Zetterberg et al., 2008; Ahmed et al., 2010). However, the details of the mechanism underlying the βCTF mediated endosomal anomalies remain unclear.

Previously, we identified TMEM30A (CDC50A), a subcomponent of lipid flippases, as a candidate partner for βCTF. This complex mediates the formation of enlarged endosomes (Takasugi et al., 2018). Most lipid flippases consist of TMEM30A and active subcomponents, P4-ATPases. These enzymes translocate phospholipids from the exoplasmic/luminal side to the cytoplasmic leaflet of the lipid bilayer to regulate phospholipids asymmetry (Andersen et al., 2016).

Phosphatidylserine (PS), one of the phospholipids, is a component of lipid bilayer and mainly localizes at the cytoplasmic leaflet (Andersen et al., 2016). PS level on the cytosolic side in endosomes determines the recruitment of PS-binding proteins to trigger membrane budding, which promotes subsequent vesicle fission and transport (Leventis and Grinstein, 2010; Varga et al., 2020). This PS asymmetry is regulated by one of the endosomal lipid flippases, those composed of TMEM30A and active subcomponent ATP8A1,

[1]Department of Medicinal Pharmacology, Graduate School of Medicine, Dentistry and Pharmaceutical Sciences, Okayama University, 1-1-1 Tsushima-naka, Kita-ku, Okayama 700-8530, Japan

[2]Research Fellow of Japan Society for the Promotion of Science, Chiyoda-ku, Tokyo 102-0083, Japan

[3]Department of Cellular and Molecular Pharmacology, Juntendo University Graduate School of Medicine, 2-1-1 Hongo Bunkyo-ku, Tokyo 113-8421, Japan

[4]Department of Neurocognitive Science, Nagoya City University Graduate School of Medical Sciences, Nagoya, Aichi, Japan

[5]Laboratory for Proteolytic Neuroscience, RIKEN Center for Brain Science, Wako, Saitama, Japan

[6]Laboratory of Neuropathology and Neuroscience, Graduate School of Pharmaceutical Sciences, The University of Tokyo, Tokyo 113-0033, Japan

[7]Department of Neuropathology, Graduate School of Medicine, The University of Tokyo, 7-3-1 Hongo Bunkyo-ku, Tokyo, 113-0033, Japan

[8]Lead contact

*Correspondence: ntakasu@okayama-u.ac.jp

https://doi.org/10.1016/j.isci.2022.103869

This is an open access article under the CC BY-NC-ND license (http://creativecommons.org/licenses/by-nc-nd/4.0/).

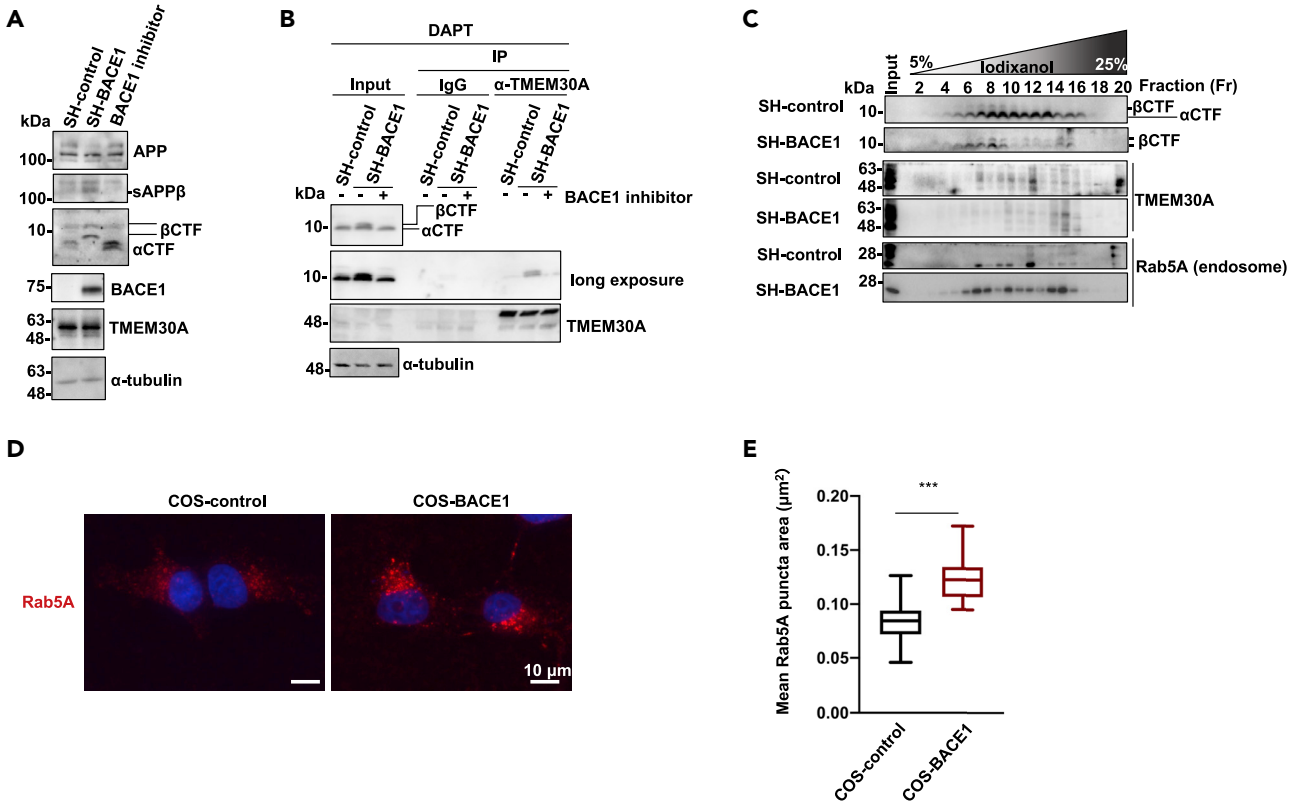

Figure 1. BACE1 upregulation induces the complex formation between TMEM30A and βCTF and endosomal anomalies

(A) Immunoblotting analysis for APP metabolites and TMEM30A in SH-control and SH-BACE1 cells. sAPPβ in the cultured media was analyzed. β-secretase inhibitor IV (10 μM) was treated to SH-BACE1 cells.

(B) Co-immunoprecipitation analysis using TMEM30A antibody in the accumulation of βCTF by the DAPT (10 μM) treatment or co-treatment with β-secretase inhibitor IV (10 μM) for 24 h.

(C) Iodixanol gradient fractionation of the homogenates from SH-control and SH-BACE1 cells. For the endosome marker, Rab5A was used.

(D) COS-control and COS-BACE1 cells were immunostained for Rab5A (Red). DAPI stained the nucleus (Blue). Scale bars: 10 μm. Representative z stack images were captured using a 60x objective lens (zoom x2.6).

(E) Quantitation of the mean area of Rab5A positive puncta. Graph shows boxplot of the mean value in each field of view in total experiments. The bar in the box: median; whiskers: Min to Max (n = 30: 10 fields × three trials, two-tailed Student's t-test, ***$p < 0.001$).

which has a high affinity for PS (Andersen et al., 2016). These lines of evidence indicate that lipid flippase activity is essential for vesicular trafficking.

In this study, we investigated whether lipid flippase activity contributes to the βCTF-mediated endosomal anomalies and could be a therapeutic target for AD treatment.

RESULTS

BACE1 upregulation promotes complex formation between endogenous TMEM30A and accumulated βCTF and endosomal anomalies

To gain insight into the early pathology of AD, we established BACE1 stably overexpressing SH-SY5Y cell lines (SH-BACE1 cells). BACE1 produces β1 or β11CTF depending on APP cleavage sites (Deng et al., 2013). BACE1 upregulation increased the β-secretase products sAPPβ, βCTF, and Aβ, although it severely reduced α-secretase-cleaved carboxyl-terminal fragment (αCTF), in good agreement with previous reports (Vetrivel et al., 2011) (Figures 1A and S1A). We previously demonstrated that TMEM30A is a candidate partner for βCTF (β1/β11CTF)-mediated endosomal anomalies (Takasugi et al., 2018). Supportively, CFP-TMEM30A, SC100 (Iwata et al., 2001), and SC89 (artificial β1 and β11CTF) co-transfection revealed that TMEM30A could interact with these βCTF (Figure S1B). Although βCTF in non-treated SH-BACE1 cells might deserve further analysis, we found that endogenous βCTF exhibited resistance to mild detergents

such as CHAPS (Figures S1C and S1D). Indeed, βCTF insolubility in mild detergents was reported elsewhere (Sakurai et al., 2008). Our result suggests that the environment surrounding βCTF is particularly unique. Therefore, to verify whether endogenous TMEM30A interacts with accumulated βCTF in SH-BACE1 cells, we treated γ-secretase inhibitor DAPT to accumulate APP-CTF, and then performed co-immunoprecipitation analysis. In line with our previous findings, we observed an interaction between the endogenous TMEM30A and accumulated βCTF, but not αCTF, and the BACE1 inhibitor co-treatment abolished this interaction (Figure 1B).

Next, a stepwise iodixanol gradient organelle fractionation was performed as described previously (Lee et al., 2003) to analyze the protein distributions. The distribution of LAMP2 (lysosome marker) and calreticulin (ER marker) showed no obvious change between SH-control and SH-BACE1 cells (Figure S2A). In contrast, Rab5A, an early endosome marker, was distributed in fractions (Fr) 7-12 in SH-control cells (Figure 1C) and its distribution was broadened to the heavier fractions (Fr 14-16) in SH-BACE1 cells. Similarly, βCTF, enriched in Fr six to nine in SH-control cells, changed its distribution in the heavier fractions (Fr 14-16) in SH-BACE1 cells (Figure 1C). Concomitantly, BACE1 was distributed in Fr 14-16 in SH-BACE1 cells (Figure S2A). Intriguingly, TMEM30A was mainly distributed in Fr 7-12 in SH-control cells. However, in SH-BACE1 cells, its distribution drastically changed to Fr 14-16 where Rab5, βCTF, and BACE1 abnormally co-localized (Figure 1C). We observed no alteration in the TMEM30A and Rab5A protein levels between SH-control and SH-BACE1 cells (Figures 1A and S2B).

Next, we performed immunofluorescence analysis using BACE1 stably overexpressing COS-7 cells (COS-BACE1), well-characterized in organelle morphology observations (Takasugi et al., 2018; Lee et al., 2015; Matsudaira et al., 2017). In contrast to the lack of alteration in the Rab5A protein level (Figure S2C), the mean of the Rab5A positive puncta area and the frequency of size distribution (0.5-3.0 μm^2) were significantly increased in COS-BACE1 cells (Figures 1D, 1E, and S2D). Although the number of trials is smaller than other analyses, we also confirmed that BACE1 inhibitors tended to suppress the increased mean of the Rab5A positive puncta area in COS-BACE1 cells (Figure S2E).

We confirmed that each cell in SH-BACE1 and COS-BACE1 shows comparable expression level (Figure S2F).

Thus, our findings suggest that BACE1 increases βCTF level, which interacts with TMEM30A and mediates endosomal anomalies.

βCTF accumulation triggers the lipid flippase activity impairment

TMEM30A interacts with active subunits, P4-ATPases, to form lipid flippase, and contributes to stability, distribution, and activity of P4-ATPases (Andersen et al., 2016; Coleman and Molday, 2011). Therefore, we hypothesized that lipid flippase activity is associated with TMEM30A/βCTF-mediated endosomal anomalies.

Immunoprecipitation analysis in the membrane fractions revealed that the physiological complex formation between TMEM30A and ATP8A1, an endosomal P4-ATPase which has a high affinity for PS, significantly decreased in SH-BACE1 cells. The BACE1 inhibitor treatment recovered this interaction in SH-BACE1 cells (Figures 2A, 2B, and S3A), indicating that this deficit is BACE1 activity-dependent.

Because it is difficult to evaluate lipid flippase activity in organelles such as endosomes, we attempted to exploit the endosomal PS binding property of Evectin2, a promoting factor of membrane fission in vesicle transport to analyze the lipid flippase activity. Evectin-2 has a PS-specific pleckstrin-homology (PH) lipid-binding domain, and its association with the endosomal membrane depends on lipid flippase activity (Lee et al., 2012; Matsudaira et al., 2017). As previously reported (Matsudaira et al., 2017), the predominant distribution of Evectin-2 in the membrane fractions was abolished by TMEM30A knockdown (Figures 2C, 2D, and S3B). The specificity of antibody was validated by Evectin-2 knockdown (Figures S3C). Intriguingly, Evectin-2 dissociated from the membrane fractions in SH-BACE1 cells and got redistributed upon the BACE1 inhibitor treatment without altering total Evectin-2 level (Figures 2E and 2F).

To further quantify Evectin-2 localization in the endosomes, we used a NanoBiT luciferase reconstitution system. Large BiT (LgBiT) and Small BiT (SmBiT) are the parts of the *Oplophorus gracilirostris*-derived Nanoluc luciferase. As SmBiT has a low affinity (Kd = 190 μM) to the LgBiT, their interaction is fragile and reversible, and the luciferase activity is not reconstituted without their forced proximity by fused proteins (Dixon et al., 2016). We fused these subunits to Rab5A (LgBiT-Rab5) and Evectin-2 (SmBiT-Evectin-2)

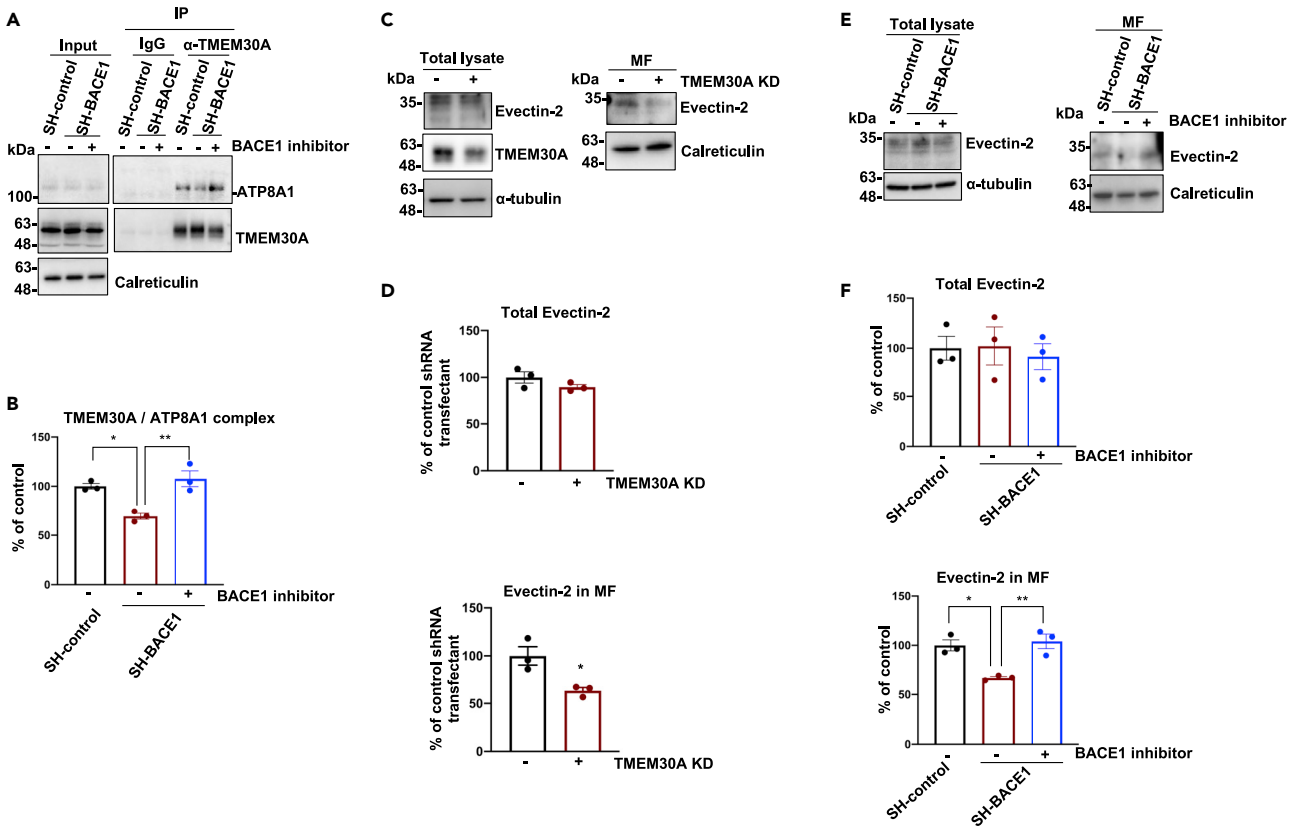

Figure 2. BACE1 upregulation induces lipid flippase dysfunction depending on the BACE1 activity

(A) The membrane fractions from SH-control and SH-BACE1 cells applied to co-immunoprecipitation analysis using TMEM30A antibody. Cells were treated with the β-secretase inhibitor IV (10 μM) for 48 h. Calreticulin was used as a loading control of membrane fractions.

(B) Quantification of ATP8A1 co-immunoprecipitated by TMEM30A antibody in Figure 2A (n = 3, mean ± SEM, one-way ANOVA Bonferroni's multiple comparisons test, *p < 0.05, **p < 0.01).

(C) Immunoblotting analysis for Evectin-2 in total cell lysates and membrane fractions (MF) in the knockdown of TMEM30A in SH-SY5Y cells.

(D) Quantification of Evectin-2 localization in whole cell lysates or MF (n = 3, mean ± SEM, two-tailed Student's t-test, *p < 0.05).

(E) Immunoblotting analysis for Evectin-2 in total cell lysates and MF in the treatment of the β-secretase inhibitor IV (10 μM) for 48 h. (F) Quantification of the Evectin-2 localization in total lysates or MF (n = 3, mean ± SEM, one-way ANOVA Bonferroni's multiple comparisons test, *p < 0.05, **p < 0.01).

to monitor the Evectin-2 localization in the endosomes (Figure 3A). Immunofluorescence analysis showed that LgBiT-Rab5 localized in the endosomes (Figure S4A). Moreover, similar to our biochemical analysis (Figures 2C and 2D), TMEM30A knockdown significantly decreased the luciferase activity (Figures 3B, 3C, and S4B). For further validation, we investigated the effect of Evectin-2 mutant on the PH domain (K20E), lacking the binding affinity to PS (Matsudaira et al., 2017). We observed significantly reduced luciferase activity in the K20E mutant (Figures S4C and S4D). These results clearly show that our reporter system could be used for semiquantitative estimation of lipid flippase activity in endosomes.

Next, we applied this system to SH-BACE1 cells. Intriguingly, we observed a significant reduction in the lipid flippase activity, rescued by the BACE1 inhibitor treatment (Figures 3D and 3E). To confirm that the BACE1-mediated APP cleavage is a prerequisite for this event, we performed APP knockdown in SH-BACE1 cells and detected lipid flippase activity recovery (Figures 3F, 3G, and S5A–S5C). Interestingly, the APP knockdown didn't affect the lipid flippase activity in SH-control cells (Figure S5D). Our data indicate that the decrease in lipid flippase activity does not occur by APP metabolites in physiological conditions but is triggered by an increase in BACE1 activity. Furthermore, lipid flippase activity significantly decreased in SC100 stably overexpressing SH-SY5Y cells (Figures 3H and 3I).

Our data strongly support the hypothesis that βCTF accumulation leads to lipid flippase dysfunction via abnormal complex formation with TMEM30A.

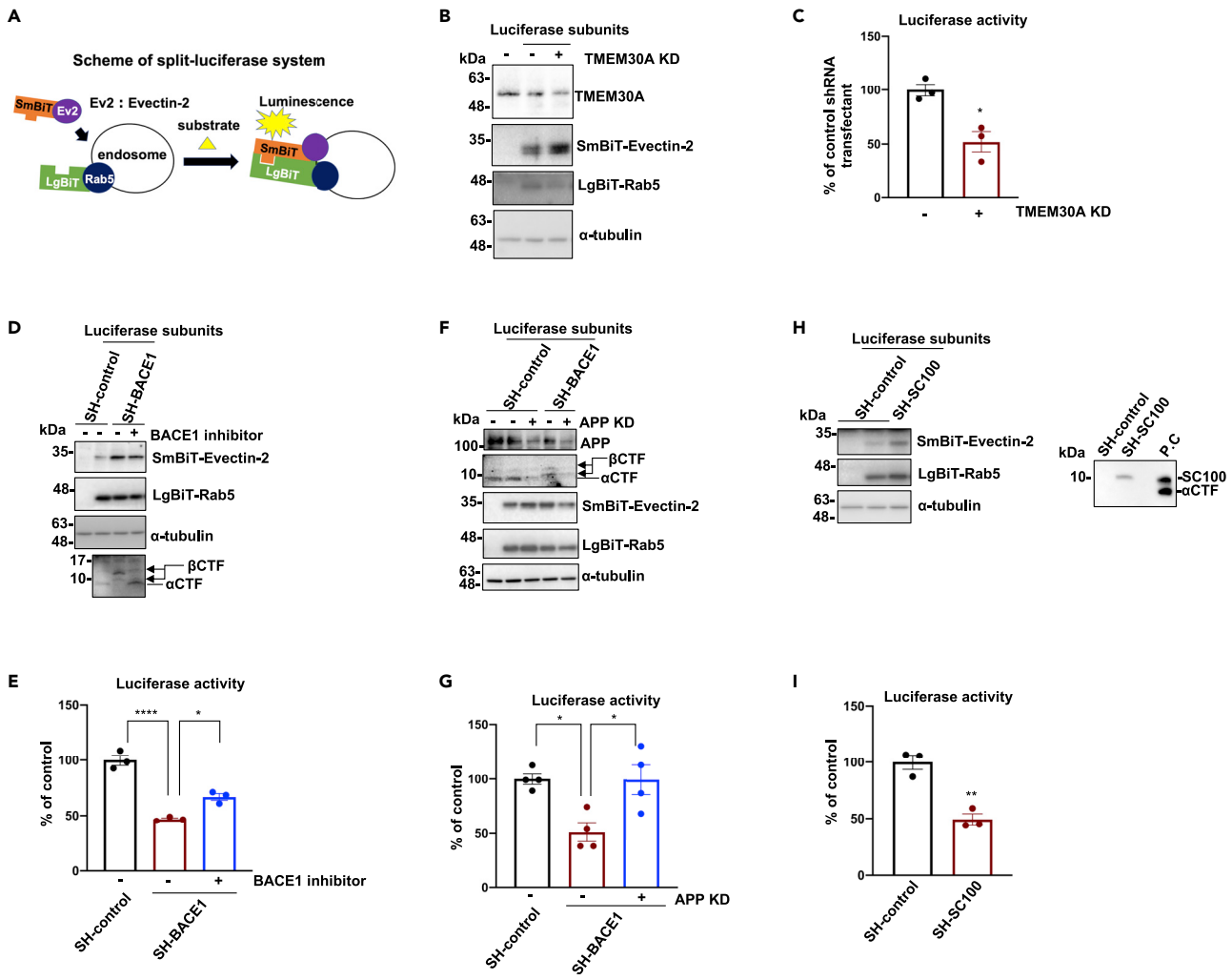

Figure 3. The semi-quantitative analysis shows the lipid flippase activity in endosomes is decreased depending on the levels of βCTFs

(A) Schematic view of the measurement methods for endosomal lipid flippase activity using a split-luciferase assay system. Luciferase subunits, LgBiT or SmBiT, were fused with Rab5A or Evectin-2, respectively. The reconstitution of luciferase activity depends on the endosomal distribution of Evectin-2, which reflects the endosomal lipid flippase activity (Figure 2).

(B) Immunoblotting analysis for LgBiT-Rab5, SmBiT-Evectin-2, and TMEM30A using HA, FLAG, and TMEM30A antibodies in the knockdown of TMEM30A for 72 h in SH-SY5Y cells.

(C) Quantification of the luciferase activity by the interaction between SmBit-Evectin2 and LgBit-Rab5 in SH-SY5Y cells with 72 h knockdown of TMEM30A. (n = 3, mean ± SEM, two-tailed Student's t-test, *$p < 0.05$).

(D) Immunoblotting analysis for LgBiT-Rab5, SmBiT-Evectin-2, and APP-CTF in the treatment of β-secretase inhibitor IV (10 μM) for 48 h.

(E) Quantification of the luciferase activity for treating β-secretase inhibitor IV (10 μM) for 48 h (n = 3, mean ± SEM, one-way ANOVA Bonferroni's multiple comparisons test, *$p < 0.05$, ****$p < 0.0001$).

(F) Immunoblotting analysis for LgBiT-Rab5, SmBiT-Evectin-2, APP, and APP-CTF in the knockdown of APP for 72 h.

(G) Quantification of the luciferase activity in the knockdown of APP for 72 h (n = 4, mean ± SEM, one-way ANOVA Bonferroni's multiple comparisons test, *$p < 0.05$). (H) Immunoblotting analysis for SC100, LgBiT-Rab5, and SmBiT-Evetin-2. P.C is the control for SC100 and αCTF.

(I) Quantification of the luciferase activity in SH-control and SH-SC100 cells 48 h after the transfection of luciferase subunits (n = 3, mean ± SEM, two-tailed Student's t-test, **$p < 0.01$).

TMEM30A/βCTF complex formation and subsequent lipid flippase dysfunction precede Aβ deposition in AD model mice

Next, we explored the TMEM30A/βCTF complex formation and lipid flippase dysfunction at the early stage in AD model mice. As A7 model mice show a relatively slow Aβ deposition, starting at approximately 9 months of age, we used these AD model mice as an appropriate model to observe the precursory phenomenon (Yamada et al., 2009). At 3 and 6 months, the ATP8A1, TMEM30A, and Evectin-2 protein levels

were not significantly different between the WT and transgenic (Tg) mice (Figures S6A and S6B). Moreover, we observed no significant difference in the αCTF and βCTF levels between the three- and 6-month-old Tg mice (Figures S6A and S6B). Intriguingly, TMEM30A interacted with βCTF in both three- and 6-month-old model mice (Figures 4A and 4B). However, TMEM30A failed to interact with Aβ oligomers, previously described as another factor in vesicular traffic impairment (Umeda et al., 2015), and with Aβ monomers (Figure S7). Importantly, both lipid flippase formation (Figures 4A and 4C) and Evectin-2 localization in the membrane fractions (Figures 4A and 4D) significantly decreased in 6-month-old A7 mice. We confirmed that the indicated band is Evectin-2 (Figure S6C). Our results suggest that the TMEM30A/βCTF complex induces lipid flippase dysfunction, which precedes Aβ deposition. Next, we analyzed other AD model mice, $App^{NL-G-F/NL-G-F}$ knock-in mice (Saito et al., 2014). This model allows us to analyze APP under endogenous expression level and exclude the artifact of overexpression. Intriguingly, TMEM30A interacted with βCTF in 3-month-old $App^{NL-G-F/NL-G-F}$ mice (Figures 4E and 4F). Concomitantly, lipid flippase formation of TMEM30A and ATP8A1 was significantly decreased (Figures 4E and 4G). Although not significant ($p = 0.08$), Evectin-2 localization in membrane fractions shows decreased trend (Figures 4E and 4H). These results strongly support the hypothesis that lipid flippase dysfunction is not an artifact of APP overexpression and mediated by TMEM30A/βCTF complex derived from the accumulation of βCTF.

βCTF/Aβ interactive peptide "T-RAP" improves endosome enlargement

We expected that the inhibition of the interaction between TMEM30A and βCTF could improve lipid flippase dysfunction and endosomal anomalies. Previously, we identified that the extracellular domain of TMEM30A (TmEx) interacts with the Aβ sequence of βCTF (Takasugi et al., 2018). We explored the interacting domain by sequential deletion of TmEx using GST-pulldown assay (Figures 5A–5C) and found that the 117–166 AA region contains the critical residues for the interaction with βCTF (Figures 5B–5D). Using RaptorX prediction (http://raptorx.uchicago.edu/), we noticed that the conformation of the α-helices and β-sheet exists in the well-conserved 125–150 AA region. We named this sequence "T-RAP" (Tmem30A related amyloid-beta interacting peptide) (Figure 5A). We verified that GST-fused T-RAP efficiently pulled down βCTF and Aβ, but not αCTF (Figures 5B, 5D, and S8), indicating T-RAP has a high affinity for Aβ N-terminal sequence.

To assess whether the synthetic T-RAP peptide influences lipid flippase activity, we treated SH-SY5Y cells with T-RAP and performed a flippase activity assay. In advance, we confirmed that T-RAP displayed no toxicity at the density used in this study (Figure S9A). Although not significant, T-RAP showed a trend to improve lipid flippase activity in SH-BACE1 cells (Figures 6A and 6B). On the other hand, T-RAP (50 μM) fused with the Trans-Activator of Transcription Protein (TAT) at N-terminal which is easily introduced into cells significantly rescued the lipid flippase activity in SH-BACE1 cells (Figure S9B). We consider that TAT-T-RAP could penetrate membranes more efficiently than T-RAP.

As lipid flippase dysfunction is βCTF level-dependent, we investigated the involvement of T-RAP in APP metabolism. After a 48 h T-RAP peptide treatment, the sAPPβ and βCTF levels significantly decreased without altering the full-length APP and TMEM30A protein levels (Figures 6C and 6D). Next, we analyzed the T-RAP effect on endosomal morphology in COS-7 cells. Importantly, T-RAP significantly decreased the mean of the Rab5A positive puncta area and the frequency of size distribution (1.0-5.0 μm2) in COS-BACE1 cells without altering the total Rab5A protein level (Figures 6E, 6F, S9C, and S9D).

These lines of evidence explain that T-RAP peptide improves endosomal anomalies by rescuing the lipid flippase activity.

DISCUSSION

βCTF-mediated endosomal anomalies in forming enlarged endosomes are considered early AD pathogenic events (Kim et al., 2016). In this study, we showed that lipid flippase activity in endosomes decreased by elevated βCTF level and it contributes to endosomal anomalies. Moreover, in the AD model mice brain, age-dependent lipid flippase dysfunction occurs before Aβ deposition, supporting their strong link with the early pathogenic event. Importantly, we found that the βCTF/Aβ-interacting peptide "T-RAP" could recover the lipid flippase activity and endosomal anomalies. Therefore, our findings suggest that lipid flippase impairment is a driving mechanism of βCTF-mediated endosomal anomalies and present a therapeutic strategy for AD treatment.

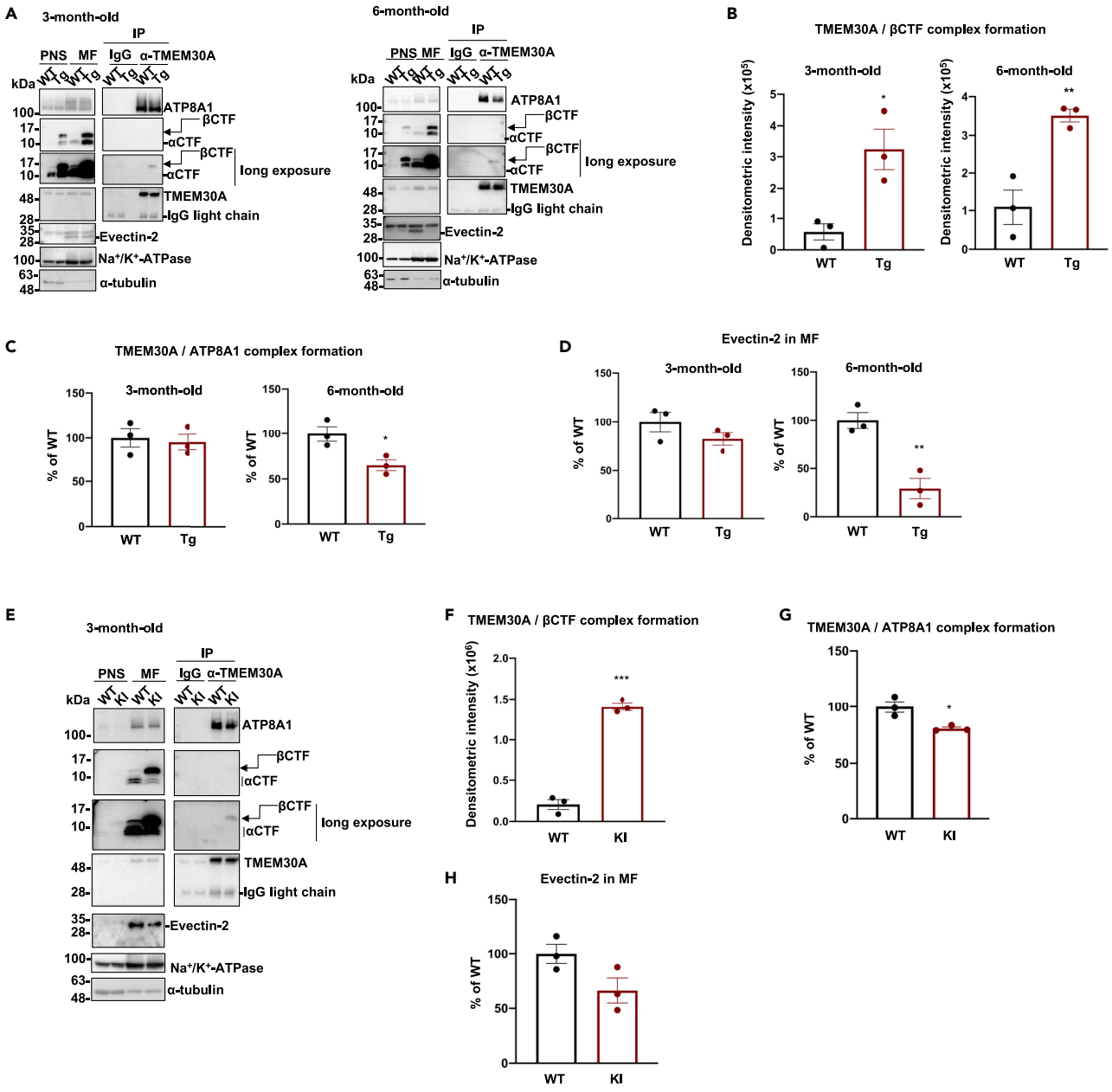

Figure 4. TMEM30A interacts with βCTF in AD model mice, which follows by lipid flippase dysfunction

(A) The membrane fractions from WT and Tg (A7) mice brain at three- or 6-month-old applied to co-immunoprecipitation analysis using TMEM30A antibody. Na^+/K^+-ATPase was used as a loading control of membrane fractions.

(B and C) Quantification of the complex formation of (B) TMEM30A and βCTF or (C) TMEM30A and ATP8A1 ($N = 3$, n = 3, mean ± SEM, two-tailed Student's t-test, *p < 0.05, **p < 0.01).

(D) Quantification of Evectin-2 localization in membrane fractions ($N = 3$, n = 3, mean ± SEM, two-tailed Student's t-test, **p < 0.01).

(E) The membrane fractions from WT and KI ($App^{NL-G-F/NL-G-F}$) mice brain at 3-month-old applied to co-immunoprecipitation analysis using TMEM30A antibody.

(F and G) Quantification of the complex formation of (F) TMEM30A and βCTF or (G) TMEM30A and ATP8A1. ($N = 3$, n = 3, mean ± SEM, two-tailed Student's t-test, *p < 0.05, ***p < 0.001).

(H) Quantification of Evectin-2 localization in membrane fractions ($N = 3$, n = 3, mean ± SEM, two-tailed Student's t-test, p = 0.08).

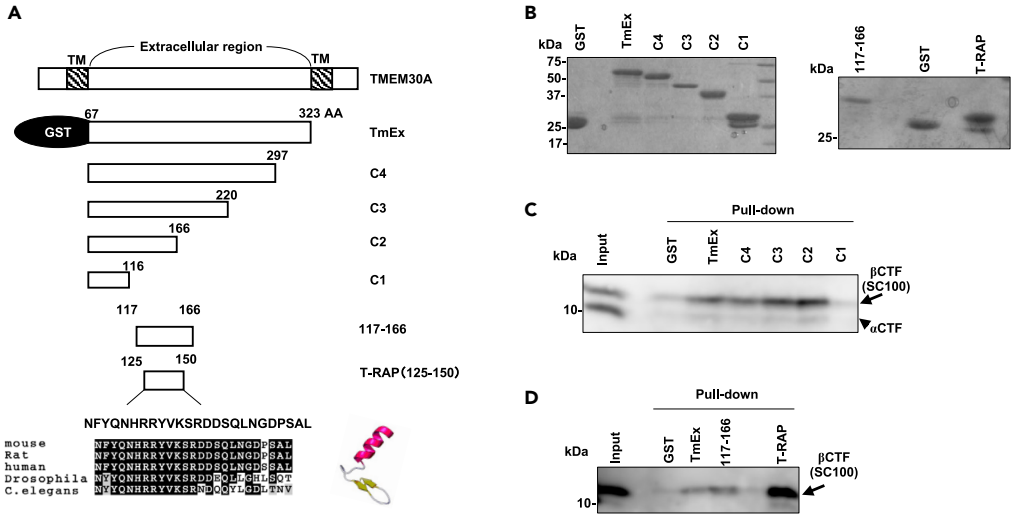

Figure 5. Identification of T-RAP peptide

(A) Schematic view of the sequential deletion constructs of GST-TmEx (Extracellular-domain of TMEM30A) and GST fused TMEM30A (117-166 AA) and "T-RAP" sequence. Lowest panel: The conservation of the T-RAP sequence among indicated species and predicted structure by Raptor-X.

(B) Coomassie's brilliant blue staining of purified GST-fusion proteins in Figure 5A.

(C and D) GST-pull down from HEK293 lysate transfected with SC100.

Endosomal anomalies are the signature for vesicular traffic impairment and could be found in the early phase of AD and Down syndrome (DS) before Aβ deposition (Cataldo et al., 2000). As DS displays trisomy on chromosome 21, upregulating APP expression, many studies have focused on APP metabolites toxicity. Among these metabolites, the BACE1 product βCTF is considered the driver for endosomal anomalies. Supportively, βCTF accumulation is observed in AD brains (Kim et al., 2016), concomitant with upregulated BACE1 expression and activity in AD brains (Ahmed et al., 2010). Several studies using human APP/Presenilin-1 familial AD mutant knock-in iPSC-derived neurons (Kwart et al., 2019) or 3xTg-AD model mice (Lauritzen et al., 2012) have shown that endosome enlargement depends on elevated βCTF but not Aβ. Moreover, analysis of DS fibroblasts or Ts65Dn model mice has demonstrated that accumulated βCTF induces endosome enlargement (Xu et al., 2016). However, the underlying mechanisms are not fully explored.

To model the early pathogenic event of AD, we established a BACE1 stably overexpressing neuroblast cell line (SH-BACE1) and observed an increase in BACE1 products, β1CTF (C99), and β11CTF (C89) (Figure 1A). Interestingly, we found that a subcomponent of lipid flippase, TMEM30A, is the interacting partner for these βCTF (Figures 1B and S1B). Concomitantly, our organelle fractionation analysis showed a broadened distribution of the endosomal marker protein Rab5A to heavier fractions (Fr 14-16) in SH-BACE1 cells compared with normal endosome fractions (Fr 7-12) in control cells. Moreover, TMEM30A, βCTF, and BACE1 were co-distributed in these abnormal heavier fractions (Figures 1C and S2A). We hypothesize the vicious cycle, in which increased βCTF triggers the interaction with TMEM30A to promote endosomal anomalies, and then the abnormal distribution of BACE1 further promotes βCTF production. In connection with these results, immunofluorescence analysis using COS-7 cells showed the formation of enlarged endosomes in COS-BACE1 cells (Figures 1D and 1E). Supportively, our previous study showed that βCTF co-localized with TMEM30A in enlarged endosomes in COS-7 cells (Takasugi et al., 2018). Another study proposed that intracellular Aβ, such as Aβ oligomers, cause vesicular traffic impairment (Umeda et al., 2015). However, we failed to detect the interaction between TMEM30A and Aβ monomers or oligomers in A7 mice (Figure S7). Although we cannot fully rule out the possibility of the Aβ oligomer involvement in a more advanced stage of AD, our data indicate that the major partner of TMEM30A, which mediates endosome enlargement, is βCTF.

There are two possible mechanisms underlying the TMEM30A/βCTF complex-mediated endosome enlargement. The first is lipid flippase dysfunction and the second is Rab5 overactivation.

Most lipid flippases consist of TMEM30A and active subcomponents, P4-ATPases (Bryde et al., 2010; Wang et al., 2018), and regulate phospholipid asymmetry in the lipid bilayer (Andersen et al., 2016). TMEM30A

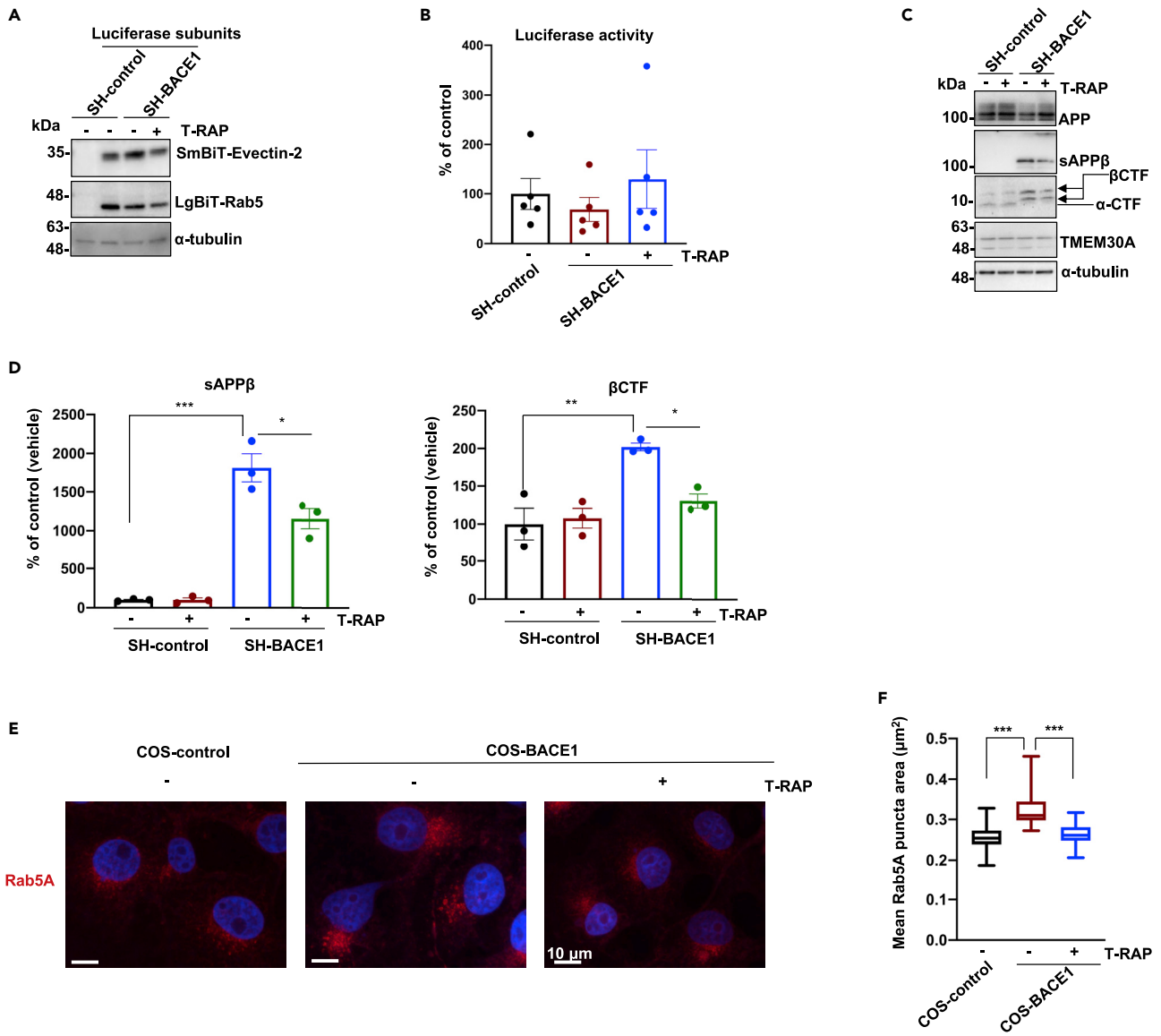

Figure 6. βCTF interacting peptide 'T-RAP' shows a trend to rescue lipid flippase activity and improves the endosomal anomalies in BACE1 upregulation

(A) Immunoblotting analysis for SmBiT-Evectin-2 and LgBiT-Rab5 after the treatment of T-RAP (10 μM) for 48h.

(B) Quantification of the luciferase activity in T-RAP (10 μM) treatment for 48 h (n = 5, mean ± SEM, one-way ANOVA Bonferroni's multiple comparisons test).

(C) Immunoblotting analysis for APP metabolites and TMEM30A in T-RAP (10 μM) treatment for 48 h sAPPβ in the cultured media was analyzed.

(D) Quantification of sAPPβ and βCTF in Figure 6C (n = 3, mean ± SEM, one-way ANOVA Bonferroni's multiple comparisons test, *p < 0.05, **p < 0.01, ***p < 0.001).

(E) COS-control and COS-BACE1 cells were immunostained for Rab5A after T-RAP (10 μM) treatment for 48 h. Scale bars: 10 μm. Representative z stack images were captured using a 60× objective lens (zoom ×2.6).

(F) Quantification of the mean Rab5A positive puncta area. Graph shows boxplot (Min to Max) of the mean value in each field of view in total experiments. The bar in the box: median; whiskers: Min to Max (n = 40: 10 fields × four trials, one-way ANOVA Bonferroni's multiple comparisons test, ***p < 0.001).

regulates proper cellular localization and activity of partners, P4-ATPases (Coleman and Molday, 2011; Van Der Velden et al., 2010). Intriguingly, we showed the complex formation of TMEM30A and ATP8A1, a brain-enriched endosomal P4-ATPase (Wang et al., 2018), decreased in SH-BACE1 cells, and the inhibition of the BACE1 activity recovered the physiological complex formation (Figures 2A and 2B). Our data suggest the hypothesis that upregulated BACE1 activity accumulates βCTF, which interacts with TMEM30A to interrupt the complex formation between TMEM30A and ATP8A1. Indeed, the age-dependent disruption of this

lipid flippase formation was followed by TMEM30A/βCTF complex formation in A7 model mice (Figures 4A–4C). These results were reproduced in 3-month-old $App^{NL-G-F/NL-G-F}$ mice (Figures 4E–4G), which shows the phenotype is not an artificial effect of APP overexpression. We consider that the TMEM30A/βCTF complex further accumulates βCTF in a vicious cycle, disrupting lipid flippase formation. Supporting this idea, TMEM30A overexpression in COS-7 cells accumulates βCTF, concomitantly with the complex formation of TMEM30A and βCTF (Takasugi et al., 2018).

Endosomal lipid flippases transport phospholipids, like PS, to the cytosolic leaflet (Andersen et al., 2016). PS on the cytosolic side in endosomes recruits PS-binding proteins, such as Evectin-2, to promote membrane fission and trigger vesicle transport (Leventis and Grinstein, 2010; Varga et al., 2020). In this study, we focused on Evectin-2 distribution in the endosomes to indirectly monitor lipid flippase activity. We clarified that Evectin-2 distribution decreased depending on the increased βCTF level in SH-BACE1 cells using biochemical analysis (Figure 2) and the split-luciferase system (Figure 3). These findings suggest that accumulated βCTF decreases the lipid flippase activity in endosomes to reduce PS level on the cytosolic side. Moreover, the A7 model mice analysis indicated decreased Evectin-2 distribution in the membrane fractions (Figures 4A and 4D). Although it was not significant, a similar trend was observed in 3-month-old $App^{NL-G-F/NL-G-F}$ mice (Figures 4E and 4H). It will be necessary to observe whether aging accelerates the decline in the activity of lipid flippases as future analysis. Indeed, the ATP8A1 knockdown induces endosome-mediated membrane traffic defects (Lee et al., 2015). Therefore, we propose the hypothesis that the TMEM30A/βCTF complex impairs lipid flippase formation and its activity to develop endosomal anomalies. It is important to note that our split-luciferase system can be applied to various organelle markers to estimate the localization of proteins and may be developed into a semiquantitative method for measuring vesicular trafficking. Further validation is needed as a future study.

The second possible mechanism is Rab5 activation. Previous reports, using Rab5A constitutively active mutant (Q79L) (Wegener et al., 2010) and overexpressing mice (Pensalfini et al., 2020), showed Rab5 positive enlarged endosomes. In addition, elevated βCTF can form a complex with APPL1, a Rab5 effector protein, which mediates Rab5 activation and endosome enlargement in DS fibroblasts and AD brains (Kim et al., 2016). Consistent with these reports, we observed the upregulation of BACE1 mediated the abnormal co-distribution of Rab5A and βCTF to alter Rab5A positive endosomal morphology (Figures 1C–1E). Therefore, accelerated βCTF accumulation by its complex formation with TMEM30A might activate Rab5 to induce endosome enlargement. It would deserve further investigation that lipid flippase dysfunction contributes to Rab5 activation-dependent or independent endosomal anomalies.

Questions still remain concerning how lipid flippase-mediated endosomal anomalies could contribute to AD pathogenesis. Previously, APP-dependent endosomal anomalies and the traffic impairment of nerve growth factor (NGF), which resulted in neuronal atrophy, were observed in rodent neuron models (Xu et al., 2016). Another study demonstrated that TMEM30A deficiency influenced sAPPβ and βCTF levels, as well as Aβ/p3 production via the increased β/α-secretase processing of APP (Tambini and D'Adamio, 2020). Therefore, lipid flippase dysfunction possibly mediates APP metabolic changes or vesicle transport deficit such as NGF to contribute to AD pathogenesis.

Because vesicular traffic impairment has been implicated as the contributor of AD pathology, βCTF-mediated endosomal anomalies might be promising therapeutic targets for treating AD. The BACE1 inhibitor might be a candidate. According to this notion, β-secretase inhibitor IV recovered lipid flippase function (Figures 2E, 2F, and 3E). However, the study of BACE1 knockout mice showed unexpected neuronal phenotypes, such as schizophrenia endophenotypes, or spine density reduction, originating from abrogated β-secretase processing of different substrates such as neuregulin 1 (NRG1) (Vassar, 2014; Savonenko et al., 2008). Further therapeutic candidates are pharmacological chaperons to stabilize retromers and limit APP processing in the endosomes by enhancing vesicle transport (Mecozzi et al., 2014). There is also a concern that the compound displays a too wide effect range and side effects (Berman et al., 2015). These lines of evidence remind us to develop more specific therapeutic targets reflecting AD pathology.

We observed a progressive decline of lipid flippase function in AD model mice (Figures 4A, 4D, 4E, and 4H). Moreover, a genome-wide association study identified AD risk variants in one of the P4-ATPases, *ATP8B4* (Holstege et al., 2020). Therefore, lipid flippase dysfunction could be associated with AD pathogenesis and

the optimal target based on AD pathology. Intriguingly, we identified a TMEM30A-derived peptide, "T-RAP," specifically interacting βCTF and Aβ. T-RAP tended to rescue the lipid flippase activity and improved endosome enlargement in BACE1 stably overexpressing cells (Figures 6B, 6E, 6F, and S9B). We hypothesize that T-RAP enfolds βCTF to inhibit the interaction with TMEM30A, and then recovers the lipid flippase physiological formation and activity. This functional lipid flippase recovery could prevent βCTF-mediated endosomal anomalies, enhancing vesicle transport (Figure 6E and 6F). T-RAP also decreased sAPPβ and βCTF levels (Figures 6C and 6D), which means the peptide corrects vesicle transport to normalize APP processing. Another possibility is that T-RAP directly binds to the proximal site of BACE1 cleavage of APP. Moreover, T-RAP is hydrophilic and easy to handle biochemically. Although further T-RAP specificity analyses would be required, we propose that T-RAP and related molecules might be the optimal candidates for AD therapeutics.

Three main problems could be distinguished in AD treatment from the perspective of vesicular traffic impairment. First, the details of the mechanisms underlying the endosomal anomalies were unclear. Second, the effective measurement of vesicular trafficking has not been established. Third, endosomal anomaly-related drug treatment has not yet been developed. In this study, we propose lipid flippase dysfunction as a mechanistic contributor for βCTF-mediated endosomal anomalies. Next, our split-luciferase system for measuring endosomal lipid flippase activity could be used for the development of quantitative vesicle transport measurements. Finally, we identified a therapeutic candidate for βCTF-mediated endosomal anomalies. Therefore, we present new insights into AD treatment for targeting the early pathogenesis, endosomal anomalies.

Limitations of the study

Several issues remain. First, we have shown that lipid flippase dysfunction depends on the level of APP metabolite by such as APP knockdown, and this result would be reinforced by analyzing the lipid flippase activity in deletion of APP metabolites by the knockout of APP. Second, the extent to which endosomal anomalies, mediated by lipid flippase dysfunction, contribute to the pathogenesis of AD is still unknown. It is necessary to analyze the interaction between βCTF and TMEM30A and Lipid Flippase activity using patient brains and neurons from patient-derived iPS cells. Third, the detailed mechanisms of improvement of endosomal anomalies by T-RAP, and its therapeutic efficacy on AD remain issues to be addressed. Further analysis of T-RAP expects to enable us to identify compounds that exhibit similar effects with T-RAP. Finally, we have developed a simple method to indirectly measure the PS level in the cytosolic side of endosomes. This method should be supported by the development of a direct measurement for the PS localization in the cytosolic side, and its applicability to measure the efficiency of protein localization should be investigated.

STAR★METHODS

Detailed methods are provided in the online version of this paper and include the following:

- KEY RESOURCES TABLE
- RESOURCE AVAILABILITY
  - Lead contact
  - Materials availability
  - Data and code availability
- EXPERIMENTAL MODEL AND SUBJECT DETAILS
  - Mice
  - Cell culture
- METHOD DETAILS
  - Plasmids, antibodies, and reagents
  - Transfection and reagents treatments
  - Alamar blue assay
  - Preparation of membrane fractions from cells and mouse brains
  - Co-immunoprecipitation
  - GST pull-down
  - Iodixanol gradient fractionation
  - Immunoblotting
  - Immunofluorescence

- Split-luciferase assay
- Aβ immunoprecipitation by 4G8 antibody
- Preparation of synthetic Aβ oligomer

- QUANTIFICATION AND STATISTICAL ANALYSIS

SUPPLEMENTAL INFORMATION

Supplemental information can be found online at https://doi.org/10.1016/j.isci.2022.103869.

ACKNOWLEDGMENTS

We are grateful to Dr. N. Nukina (Doshisha University) and the Legend research grant in 2019 for providing research materials. This work was supported by the Grant-in-Aid for Scientific Research (C) from the Japan Society for the Promotion of Science (17K08272 and 20K07014), Research Grant from the Ryobi Teien Memorial Foundation, Life Science Foundation of Japan (N. T), Grant-in-Aid for Scientific Research (C) (20K07765 to Y. K), Grant-in-Aid for Scientific Research (B) (21H02815 to T. S), Grants-in-aid for Scientific Research (A) (119H01015 to T. T), Strategic Research Program for Brain Sciences from the Japan Agency for Medical Research and Development (JP21dm0207073 to T. T), and Grant-in-Aid for JSPS Fellows (N.K).

AUTHOR CONTRIBUTIONS

N.K. and N.T. designed the research; N.K., R.I., M.K., A.I., Y.K, and N.T. performed the experiments and analyzed data; T.H. and T.S. prepared animal samples and provided antibodies, respectively; T.T. provided research materials; N.K. and N.T. wrote the paper; Y.K., T.H., T.I., T.T., T. Saito., TC. S., T. Sakurai., and T.U. provided advice and helped write the article. All authors read and approved the final manuscript.

DECLARATION OF INTERESTS

The authors declare no competing interests.

Received: August 31, 2021
Revised: December 27, 2021
Accepted: February 1, 2022
Published: March 18, 2022

REFERENCES

Ahmed, R.R., Holler, C.J., Webb, R.L., Li, F., Beckett, T.L., and Murphy, M.P. (2010). BACE1 and BACE2 enzymatic activities in Alzheimer's disease. J. Neurochem. *112*, 1045–1053. https://doi.org/10.1111/j.1471-4159.2009.06528.x.

Andersen, J.P., Vestergaard, A.L., Mikkelsen, S.A., Mogensen, L.S., Chalat, M., and Molday, R.S. (2016). P4-ATPases as phospholipid flippases-structure, function, and enigmas. Front Physiol. *7*, 275. https://doi.org/10.3389/fphys.2016.00275.

Berman, D.E., Ringe, D., Petsko, G.A., and Small, S.A. (2015). The use of pharmacological retromer chaperones in Alzheimer's Disease and other endosomal-related disorders. Neurotherapeutics *12*, 12–18. https://doi.org/10.1007/s13311-014-0321-y.

Bryde, S., Hennrich, H., Verhulst, P.M., Devaux, P.F., Lenoir, G., and Holthuis, J.C.M. (2010). CDC50 proteins are critical components of the human class-1 P4-ATPase transport machinery. J. Biol. Chem. *285*, 40562–40572. https://doi.org/10.1074/jbc.M110.139543.

Cataldo, A.M., Peterhoff, C.M., Troncoso, J.C., Gomez-Isla, T., Hyman, B.T., and Nixon, R.A. (2000). Endocytic pathway abnormalities precede amyloid β deposition in sporadic Alzheimer's disease and down syndrome: differential effects of APOE genotype and presenilin mutations. Am. J. Pathol. *157*, 277–286. https://doi.org/10.1016/S0002-9440(10)64538-5.

Coleman, J.A., and Molday, R.S. (2011). Critical role of the β-subunit CDC50A in the stable expression, assembly, subcellular localization, and lipid transport activity of the P4-ATPase ATP8A2. J. Biol. Chem. *286*, 17205–17216. https://doi.org/10.1074/jbc.m111.229419.

Deng, Y., Wang, Z., Wang, R., Zhang, X., Zhang, S., Wu, Y., Staufenbei, M., Cai, F., and Song, W. (2013). Amyloid-β protein (Aβ) Glu11 is the major β-secretase site of β-site amyloid-β precursor protein-cleaving enzyme 1 (BACE1), and shifting the cleavage site to Aβ Asp1 contributes to Alzheimer pathogenesis. Eur. J. Neurosci. *37*, 1962–1969. https://doi.org/10.1111/ejn.12235.

Dixon, A.S., Schwinn, M.K., Hall, M.P., Zimmerman, K., Otto, P., Lubben, T.H., Butler, B.L., Binkowski, B.F., Machleidt, T., Kirkland, T.A., et al. (2016). NanoLuc complementation reporter optimized for accurate measurement of protein interactions in cells. ACS. Chem. Biol. *11*, 400–408. https://doi.org/10.1021/acschembio.5b00753.

Hardy, J., and Selkoe, D.J. (2002). The amyloid hypothesis of alzheimer's disease: progress and problems on the road to therapeutics. Science *297*, 353–356. https://doi.org/10.1126/science.1072994.

Hashimoto, T., Fujii, D., Naka, Y., Kashiwagi-Hakozaki, M., Matsuo, Y., Matsuura, Y., Wakabayashi, T., and Iwatsubo, T. (2020). Collagenous Alzheimer amyloid plaque component impacts on the compaction of amyloid-β plaques. Acta. Neuropathol. Commun. *8*, 212. https://doi.org/10.1186/s40478-020-01075-5.

Holstege, H., Hulsman, M., Charbonnier, C., Grenier-Boley, B., Quenez, O., Grozeva, D., van Rooij, J.G.J., Sims, R., Ahmad, S., Amin, N., et al. (2020). Exome sequencing identifies rare damaging variants in the ATP8B4 and ABCA1 genes as novel risk factors for Alzheimer's disease. medRxiv. https://doi.org/10.1101/2020.07.22.20159251.

Huang, L.K., Chao, S.P., and Hu, C.J. (2020). Clinical trials of new drugs for Alzheimer disease. J. Biomed. Sci. *27*, 1–13. https://doi.org/10.1186/s12929-019-0609-7.

Iwata, H., Tomita, T., Maruyama, K., and Iwatsubo, T. (2001). Subcellular compartment and

molecular subdomain of β-amyloid precursor protein relevant to the Aβ42-promoting effects of Alzheimer mutant presenilin 2. J. Biol. Chem. *276*, 21678–21685. https://doi.org/10.1074/jbc.M007989200.

Kaneshiro, N., Imaoka, R., Komai, M., Kashiyama, T., Sakurai, T., Uehara, T., and Takasugi, N. (2018). Functional analysis of juxta- and intra-membrane domains of murine APP by genome editing in Neuro2a cells. Biochem. Biophys. Res. Commun. *501*, 1023–1028. https://doi.org/10.1016/j.bbrc.2018.05.102.

Kim, S., Sato, Y., Mohan, P.S., Peterhoff, C., Pensalfini, A., Rigoglioso, A., Jiang, Y., and Nixon, R.A. (2016). Evidence that the rab5 effector APPL1 mediates APP-βCTF-induced dysfunction of endosomes in Down syndrome and Alzheimer's disease. Mol. Psychiatry. *21*, 707–716. https://doi.org/10.1038/mp.2015.97.

Kwart, D., Gregg, A., Scheckel, C., Murphy, E.A., Paquet, D., Duffield, M., Fak, J., Olsen, O., Darnell, R.B., and Tessier-Lavigne, M. (2019). A large panel of isogenic APP and PSEN1 mutant human iPSC neurons reveals shared endosomal abnormalities mediated by APP β-CTFs, Not Aβ. Neuron *104*, 256–270. https://doi.org/10.1016/j.neuron.2019.07.010.

Lauritzen, I., Pardossi-Piquard, R., Bauer, C., Brigham, E., Abraham, J.D., Ranaldi, S., Fraser, P., St-George-Hyslop, P., Thuc, O.L., Espin, V., et al. (2012). The β-secretase-derived C-terminal fragment of βAPP, C99, but not Aβ, is a key contributor to early intraneuronal lesions in triple-transgenic mouse hippocampus. J. Neurosci. *32*, 16243–16255. https://doi.org/10.1523/JNEUROSCI.2775-12.2012.

Lee, M.S., Kao, S.C., Lemere, C.A., Xia, W., Tseng, H.C., Zhou, Y., Neve, R., Ahlijanian, M.K., and Tsai, L.H. (2003). APP processing is regulated by cytoplasmic phosphorylation. J. Cell. Biol. *163*, 83–95. https://doi.org/10.1083/jcb.200301115.

Lee, S., Uchida, Y., Emoto, K., Umeda, M., Kuge, O., Taguchi, T., and Arai, H. (2012). Impaired retrograde membrane traffic through endosomes in a mutant CHO cell defective in phosphatidylserine synthesis. Genes. Cells *17*, 728–736. https://doi.org/10.1111/j.1365-2443.2012.01622.x.

Lee, S., Uchida, Y., Wang, J., Matsudaira, T., Nakagawa, T., Kishimoto, T., Mukai, K., Inaba, T., Kobayashi, T., Molday, R.S., et al. (2015). Transport through recycling endosomes requires EHD1 recruitment by a phosphatidylserine translocase. EMBO. J. *34*, 669–688. https://doi.org/10.15252/embj.201489703.

Leventis, P.A., and Grinstein, S. (2010). The distribution and function of phosphatidylserine in cellular membranes. Annu. Rev. Biophys. *39*, 407–427. https://doi.org/10.1146/annurev.biophys.093008.131234.

Mamada, N., Tanokashira, D., Hosaka, A., Kametani, F., Tamaoka, A., and Araki, W. (2015). Amyloid β-protein oligomers upregulate the β-secretase, BACE1, through a post-translational mechanism involving its altered subcellular distribution in neurons. Mol. Brain *8*, 73. https://doi.org/10.1186/s13041-015-0163-5.

Matsudaira, T., Mukai, K., Noguchi, T., Hasegawa, J., Hatta, T., Iemura, S., Natsume, T., Miyamura, N., Nishina, H., Nakayama, J., et al. (2017). Endosomal phosphatidylserine is critical for the YAP signalling pathway in proliferating cells. Nat. Commun. *8*, 1246. https://doi.org/10.1038/s41467-017-01255-3.

Mecozzi, V.J., Berman, D.E., Simoes, S., Vetanovetz, C., Awal, M.R., Patel, V.M., Schneider, R.T., Petsko, G.A., Ringe, R., and Small, S.A. (2014). Pharmacological chaperones stabilize retromer to limit APP processing. Nat. Chem. Biol. *10*, 443–449. https://doi.org/10.1038/nchembio.1508.

Muko, R., Matsuda, H., Oikawa, M., Shin, T., Matsuda, K., Sato, H., Sunouchi, T., and Tanaka, A. (2021). Histidine-rich glycoprotein functions as a dual regulator of neutrophil activity in horses. Equine. Vet. J. *102*, 103620. https://doi.org/10.1016/j.jevs.2021.103620.

Pensalfini, A., Kim, S., Subbanna, S., Bleiwas, C., Goulbourne, C.N., Stavrides, P.H., Jiang, Y., Lee, J.H., Darji, S., Pawlik, M., et al. (2020). Endosomal dysfunction induced by directly overactivating rab5 recapitulates prodromal and neurodegenerative features of Alzheimer's Disease. Cell. Rep. *33*, 108420. https://doi.org/10.1016/j.celrep.2020.108420.

Saito, T., Matsuba, Y., Mihira, N., Takano, J., Nilsson, P., Itohara, S., Iwata, N., and Saido, T.C. (2014). Single App knock-in mouse models of Alzheimer's disease. Nat. Neurosci. *17*, 661–663. https://doi.org/10.1038/nn.3697.

Sakurai, T., Kaneko, K., Okuno, M., Wada, K., Kashiyama, T., Shimizu, H., Akagi, T., Hashikawa, T., and Nukina, N. (2008). Membrane microdomain switching: a regulatory mechanism of amyloid precursor protein processing. J. Cell. Biol. *183*, 339–352. https://doi.org/10.1083/jcb.200804075.

Salinas, M.L., Fuentes, N.R., Choate, R., Wright, R.C., McMurray, D.N., and Chapkin, R.S. (2020). AdipoRon attenuates Wnt signaling by reducing cholesterol-dependent plasma membrane rigidity. Biophys. J. *118*, 885–897. https://doi.org/10.1016/j.bpj.2019.09.009.

Savonenko, A.V., Melnikova, T., Laird, F.M., Stewart, K.-A., Price, D.L., and Wong, P.C. (2008). Alteration of BACE1-dependent NRG1/ErbB4 signaling and schizophrenia-like phenotypes in BACE1-null mice. Proc. Natl. Acad. Sci. U S A *105*, 10–15. https://doi.org/10.1073/pnas.0710373105.

Sinha, S., Anderson, J.P., Barbour, R., Basi, G.S., Caccavello, R., Davis, D., Doan, M., Dovey, H.F., Frigon, N., Hong, J., et al. (1999). Purification and cloning of amyloid precursor protein beta-secretase from human brain. Nature *705*, 537–540.

Takasugi, N., Tomita, T., Hayashi, I., Tsuruoka, M., Niimura, M., Takahashi, Y., Thinakaran, G., and Iwatsubo, T. (2003). The role of presenilin cofactors in the γ-secratase complex. Nature *422*, 438–441. https://doi.org/10.1038/nature01506.

Takasugi, N., Araya, R., Kamikubo, Y., Kaneshiro, N., Imaoka, R., Jin, H., Kashiyama, T., Hashimoto, Y., Kurosawa, M., Uehara, T., et al. (2018). TMEM30A is a candidate interacting partner for the β-carboxyl-terminal fragment of amyloid-β precursor protein in endosomes. PLoS ONE *3*, e0200988. https://doi.org/10.1371/journal.pone.0200988.

Tambini, M.D., and D'Adamio, L. (2020). Loss of CDC50A function drives Aβ/p3 production via increased β/α-secretase processing of APP. bioRxiv. https://doi.org/10.1101/2020.11.12.379636.

Tanaka, J., Miwa, Y., Miyoshi, K., Ueno, A., and Inoue, H. (1999). Construction of Epstein-Barr virus-based expression vector containing mini-OriP. Biochem. Biophys. Res. Commun. *264*, 938–943. https://doi.org/10.1006/bbrc.1999.1617.

Umeda, T., Ramser, E.M., Yamashita, M., Nakajima, K., Mori, H., Silverman, M.A., and Tomiyama, T. (2015). Intracellular amyloid β oligomers impair organelle transport and induce dendritic spine loss in primary neurons. Acta. Neuropathol. Commun. *3*, 51. https://doi.org/10.1186/s40478-015-0230-2.

Varga, K., Jiang, Z.J., and Gong, L.W. (2020). Phosphatidylserine is critical for vesicle fission during clathrin-mediated endocytosis. J. Neurochem. *152*, 48–60. https://doi.org/10.1111/jnc.14886.

Vassar, R., Bennett, B.D., Babu-Khan, S., Kahn, S., Mendiaz, E.A., Denis, P., Teplow, D.B., Ross, S., Amarante, P., Loeloff, R., et al. (1999). β-Secretase cleavage of Alzheimer's amyloid precursor protein by the transmembrane aspartic protease BACE. Science *286*, 735–741. https://doi.org/10.1126/science.286.5440.735.

Vassar, R. (2014). BACE1 inhibitor drugs in clinical trials for Alzheimer's disease. Alzheimers. Res. Ther. *6*, 1–14. https://doi.org/10.1186/s13195-014-0089-7.

Van Der Velden, L.M., Wichers, C.G.K., van Breevoort, A.E.D., Coleman, J.A., Molday, R.S., Berger, R., Klomp, L.W.J., and van de Graaf, S.F.J. (2010). Heteromeric interactions required for abundance and subcellular localization of human CDC50 proteins and class 1 P4-ATPases. J. Biol. Chem. *285*, 40088–40096. https://doi.org/10.1074/jbc.M110.139006.

Vetrivel, K.S., Meckler, X., Chen, Y., Nguyen, P.D., Seidah, N.G., Vassar, R., Wong, P.C., Fukata, M., Kounnas, M.Z., and Thinakaran, G. (2009). Alzheimer disease Aβ production in the absence of S-palmitoylation-dependent targeting of BACE1 to lipid rafts. J. Biol. Chem. *284*, 3793–3803. https://doi.org/10.1074/jbc.M808920200.

Vetrivel, K.S., Barman, A., Chen, Y., Nguyen, P.D., Wagner, S.L., Prabhakar, R., and Thinakaran, G. (2011). Loss of cleavage at β′-site contributes to apparent increase in β-amyloid peptide (Aβ) secretion by β-secretase (BACE1)-glycosylphosphatidylinositol (GPI) processing of amyloid precursor protein. J. Biol. Chem. *286*, 26166–26177. https://doi.org/10.1074/jbc.M111.260471.

Wang, J., Molday, L.L., Hii, T., Coleman, J.A., Wen, T., Andersen, J.P., and Molday, R.S. (2018). Proteomic analysis and functional characterization of P4-ATPase phospholipid flippases from murine tissues. Sci. Rep. *8*, 10795. https://doi.org/10.1038/s41598-018-29108-z.

Wegener, C.S., Malerød, L., Pedersen, N.M., Progida, C., Bakke, O., Stenmark, H., and Brech, A. (2010). Ultrastructural characterization of giant endosomes induced by GTPase-deficient Rab5. Histochem. Cell. Biol. *133*, 41–55. https://doi.org/10.1007/s00418-009-0643-8.

Xu, W., Weissmiller, A.M., White, J.A. 2nd., Fang, F., Wang, X., Wu, Y., Pearn, M.L., Zhao, X., Sawa, M., Chen, S., et al. (2016). Amyloid precursor protein-mediated endocytic pathway disruption induces axonal dysfunction and neurodegeneration. J. Clin. Invest. *126*, 1815–1833. https://doi.org/10.1172/JCI82409.

Yamada, K., Yabuki, C., Seubert, P., Schenk, D., Hori, Y., Ohtsuki, S., Terasaki, T., Hashimoto, T., and Iwatsubo, T. (2009). Aβ immunotherapy: intracerebral sequestration of Aβ by an anti-Aβ monoclonal antibody 266 with high affinity to soluble Aβ. J. Neurosci. *29*, 11393–11398. https://doi.org/10.1523/JNEUROSCI.2021-09.2009.

Yan, R., Bienkowski, M.J., Shuck, M.E., Miao, H., Tory, M.C., Pauley, A.M., Brashier, J.R., Stratman, N.C., Mathews, W.R., Buhl, A.E., et al. (1999). Membrane-anchored aspartyl protease with Alzheimer's disease β-secretase activity. Nature *402*, 533–537. https://doi.org/10.1038/990107.

Zetterberg, H., Andreasson, U., Hansson, O., Wu, G., Sankaranarayanan, S., Andersson, M.E., Buchhave, P., Londos, E., Umek, R.M., Minthon, L., et al. (2008). Elevated cerebrospinal fluid BACE1 activity in incipient alzheimer disease. Arch. Neurol. *65*, 1102–1107. https://doi.org/10.1001/archneur.65.8.1102.

STAR★METHODS

KEY RESOURCES TABLE

REAGENT or RESOURCE	SOURCE	IDENTIFIER
Antibodies		
ATP8A1 polyclonal antibody	Proteintech	Cat#21565-1-AP; RRID: AB_10734587
PLEKHB2 (Evectin-2) antibody	Novus Biologicals	Cat#NBP1-56835; RRID: AB_11026333
Na+/K+-ATPase α-subunit	Developmental Studies Hybridoma Bank	Cat#a5; RRID: AB_2166869
LAMP2 antibody	Santa Cruz Biotechnologies	Cat#sc-18822; RRID: AB_626858
calreticulin mouse monoclonal antibody	Stressgen	Cat#SPA-601; RRID: AB_10630195
Rab5A mouse monoclonal antibody	Cell Signaling Technology	Cat#46449; RRID: AB_2799303
Rab5A rabbit polyclonal antibody	Proteintech	Cat#11947-1-AP; RRID: AB_2269388
Rab4 rabbit antibody	Cell Signaling Technology	Cat#2167; RRID: AB_2253579
anti-human Amyloidβ (N) antibody (82E1)	Immuno-Biological Laboratories	Cat#10323; RRID: AB_10707424
anti-β-Amyloid 17-24 antibody (4G8)	BioLegend	Cat#800701; RRID: 2564633
anti-β-Amyloid 1-16 antibody (6E10)	BioLegend	Cat#803001; RRID: AB_2564653
anti-human BACE1 (C) antibody	Immuno-Biological Laboratories	Cat#18711; RRID: AB_2341403
anti-human sAPPβ-wild type antibody	Immuno-Biological Laboratories	Cat# 18957; RRID: AB_1630824
normal rabbit IgG	Wako Pure Chemical Industries	Cat# 148-09551
normal mouse IgG	Santa Cruz Biotechnologies	Cat# sc-2025; RRID: AB_737182
GFP monoclonal antibody	Invitrogen	Cat#A-11120; RRID: AB_221568
mouse monoclonal anti FLAG peroxidase (HRP) antibody	Sigma	Cat#A8592; RRID: AB_439702
HA tag mouse monoclonal antibody	Cell Signaling Technology	Cat#2367; RRID: AB_10691311
HA tag rabbit polyclonal antibody	Proteintech	Cat# 51064-2-AP; RRID: AB_11042321
anti α-tubulin monoclonal antibody	Wako Pure Chemical Industries	Cat# 017-25031
anti α-tubulin hFAB Rhodamine antibody	Bio-Rad	Cat# 12004166; RRID: AB_2884950
APP-C terminal (C15) antibody	gift from Dr. T. Sakurai	Takasugi et al. (2018)
TMEM30A-C terminal antibody	gift from Dr. T. Sakurai	Takasugi et al. (2018)
HRP linked anti rabbit IgG	Invitrogen	Cat# NA9340V; RRID: AB_772191
HRP linked anti mouse IgG	Invitrogen	Cat# NA9310V; RRID: AB_772193
HRP linked anti rabbit IgG, light chain specific	Jackson ImmunoResearch	Cat# 211-032-171; RRID: AB_2339149
Goat anti-mouse IgG (H+L) conjugated with Alexa Fluor 594	Invitrogen	Cat# A11005; RRID: AB_2534073
Goat anti-rabbit IgG (H+L) conjugated with Alexa Fluor 488	Invitrogen	Cat# A11008; RRID: AB_143165
Biological samples		
Brain hemispheres of A7 mice	Yamada et al. (2009)	N/A
Brain hemispheres of $App^{NL-G-F/NL-G-F}$ mice	Saito et al. (2014)	IMSR Cat# RBRC06344
Chemicals, peptides, and recombinant proteins		
β-secretase inhibitor IV	Cayman chemical	Cat# 23388; CAS: 797035-11-1
N- [N-(3, 5-difluorophenacetyl)-L-alanyl]-S-phenylglycine t-butyl ester (DAPT)	Cayman chemical	Cat#13197; CAS: 208255-80-5
Alamar Blue	Invitrogen	Cat# DAL 1025
T-RAP (NFYQNHRRYVKSRDDSQLNGDPSAL)	GenScript	This study

(*Continued on next page*)

Continued

REAGENT or RESOURCE	SOURCE	IDENTIFIER
TAT-GG-T-RAP (YGRKKRRQRRRGGNFYQNH RRYVKSRDDSQLNGDPSAL)	GenScript	This study
Synthetic Aβ40	Peptide Institute	Cat# 4307-v
Synthetic Aβ42	Peptide Institute	Cat# 4349-v
Critical commercial assays		
BCA protein assay kit	Takara	Cat# T9300A
Nano-Glo Live Cell Assay System	Promega	Cat# N2011
Experimental models: Cell lines		
Human: SH-SY5Y cells	ATCC	CRL-2266
African green monkey: COS-7 cells	ATCC	CRL-1651
Human: HEK293T	ATCC	CRL-3216
Human: HEK293	ATCC	CRL-1573
Deposited data		
Raw data of western blot, luciferase activity, and immunofluorescence in main figures are deposited on Mendeley	Mendeley Data	https://doi.org/10.17632/r9tx4v992v.2

RESOURCE AVAILABILITY

Lead contact

Further information and requests for resources and reagents should be directed to and will be fulfilled by the lead contact, Nobumasa Takasugi (ntakasu@okayama-u.ac.jp).

Materials availability

Plasmids and peptide generated in this study will be available upon the request.

Data and code availability

All data reported in this paper will be shared by the lead contact upon request.

Raw data of western blot, luciferase activity, and immunofluorescence in main figures are deposited on "Mendeley Data: https://doi.org/10.17632/r9tx4v992v.2".

This paper does not report original code.

Any additional information required to reanalyze the data reported in this paper is available from the lead contact upon request.

EXPERIMENTAL MODEL AND SUBJECT DETAILS

Mice

Transgenic mice that overexpress human APP695 harboring K670N, M671L, and T714I FAD mutations in neurons under the control of Thy1.2 promoter (A7 line) were previously generated (Yamada et al., 2009) and genotyped using specific primers (Hashimoto et al., 2020). All female A7 mice (3- or 6-month-old) were kept under SPF conditions and fed a regular diet (Oriental Yeast). The animal care and use procedures were approved by the Institutional Animal Care and Use Committees of the University of Tokyo (18-P-108). Female $App^{NL\text{-}G\text{-}F/NL\text{-}G\text{-}F}$ (Saito et al., 2014) mice (3-month-old) were maintained at a 12 h light/dark cycle (22°C, 40%–60% of humidity) with food and water available *ad libitum*. The animal care and use procedures were approved by the Institutional Animal Care and Use Committee/Ethics Committee of the Graduate School of Pharmaceutical Sciences, The University of Tokyo (protocol no. P31-11). Whole brains were

extracted from the skull, and brain hemispheres of A7 or App$^{NL-G-F/NL-G-F}$ mice and age-matched controls were prepared. Tissue samples were stored at −80°C until biochemical analysis.

Cell culture

Human neuroblastoma SH-SY5Y cells (female) or the African green monkey kidney fibroblast COS-7 cells (male) were transfected using indicated plasmids to establish stably overexpressing cell lines. Subsequently, these cells were selected using hygromycin (250 μg/mL, Fujifilm-Wako). Human embryonic kidney cell line HEK293 or HEK293T (female) and COS-7 cells were cultured at 37°C with 5% CO_2 in Dulbecco's modified Eagle's medium (DMEM, Fujifilm-Wako), and SH-SY5Y cells were maintained in DMEM/Ham's F-12 (Fujifilm-Wako). The media were supplemented with 10% fetal bovine serum, 100 units/ml penicillin, and 100 μg/mL streptomycin.

METHOD DETAILS

Plasmids, antibodies, and reagents

The antibodies, reagents are listed in the key resource table. Plasmids and oligonucleotides used in this study are listed in Table S1.

pEB-hyg-BACE1 and pEB-hyg-TO-SC100/-SC89 construction. Mouse BACE1 sequence in pMx-puro (Vetrivel et al., 2009) (kind gift from Dr. Gopal Thinakaran, USF Neuroscience Institute) was amplified using PrimeSTAR Max DNA Polymerase (Takara-Bio). PCR products were digested using SalI and BamHI and ligated into the equally digested episomal vector (Tanaka et al., 1999), pEB-hyg (Fujifilm-Wako). SC100 sequence was amplified from pcDNA3.1/hygromycin-SC100 (Iwata et al., 2001). The PCR products were introduced into pEB-hyg digested with XhoI and NotI using the NEBuilder Hifi DNA assembly mix (New England Biolab) following the manufacturer's instructions. To introduce Tetracycline inducibility, pEB-hyg-SC100 and pcDNA4 TO (Thermo Fisher) were digested using SnaBI and XhoI and then replaced the CMV promoter with CMV-TO. pEB-hyg-TO-SC89 was manufactured by PCR mutagenesis using pEB-hyg-SC100 as a template.

pEB-Puro-HA-LgBiT-mRab5. To generate N-terminally HA-tagged Large BiT sequence (HA-LgBiT), a PCR reaction was performed twice. In the 1st round, the LgBiT sequence was amplified, using CMV HaloTag-LgBiT (Promega) as the template. Using the 1st PCR product as a template, 2nd PCR was performed to allow the Gibson assembly reaction. Murine Rab5A (mRab5A) was amplified from DEST40-CFP-mRab5A. PCR products, HA-LgBiT and mRab5A, were assembled into pEB-puro digested with XhoI and BamHI using the NEBuilder Hifi DNA assembly mix.

p3xFLAG CMV10-SmBiT-Evectin-2/-K20E mutant. To generate Evectin-2 N-terminally fused with Small BiT (SmBiT) fragment, the SmBiT-Evectin-2 sequence was amplified using pEGFP-N1-Evectin-2 embedding human Evectin-2 CDS as the template. The SmBiT sequence was obtained from Promega. Using the PCR product as a template, the insert sequence was amplified to enable the Gibson assembly reaction. The PCR product inserted into the p3xFLAG-CMV10 was digested with EcoRI and NotI using the NEBuilder Hifi DNA assembly mix. K20E mutant was generated using long-PCR mutagenesis with p3xFLAG CMV10-SmBiT-Evectin-2 as the template.

pENTR-U6-shRNA vectors. The U6 promoter sequence was synthesized by Thermo Fisher Scientific and introduced into pENTR/D-TOPO (Thermo Fisher Scientific). Indicated shRNA template pairs were annealed and ligated into pENTR-U6 digested using AgeI and EcoRI.

pDEST-15-constructs. The codon sequence of the extracellular region of TMEM30A (67-323 AA: TmEx) was redesigned to reduce the use of rare codons in *E. Coli* and synthesized (Tm-EXN; Genscript). The stepwise shortening of the TmEx domain was accomplished by PCR amplification using primers listed in Table S1 using the TmEx sequence as a template. Each PCR product was cloned into the pENTR/D-TOPO vector. To make GST fusion protein, the target sequence was subcloned into pDEST-15 (Thermo Fisher Scientific).

Restriction enzymes used in this study were purchased from New England Biolabs.

All constructed plasmids and inserted sequences were verified using Sanger sequencing (GENEWIZ).

Transfection and reagents treatments

Cells at 50%–70% confluence were transfected with indicated plasmids using Lipofectamine 3,000 Transfection Reagent (Thermo Fisher Scientific) following the manufacture's protocol. For the interaction assay for TMEM30A and β1 or β11CTF, HEK293T cells were co-transfected with CFP-TMEM30A and SC100 (β1) or SC89 (β11), then subjected to co-immunoprecipitation analysis 48 h post-transfection. For TMEM30A knockdown, cells were reverse transfected with short hairpin RNA for each target inserted in the pENTR-U6 vector and incubated for 72 h. For APP knockdown, siRNA (SASI_Hs01_00185800, Sigma) was reverse transfected using Lipofectamine RNAiMAX Transfection Reagent (Thermo Fisher Scientific) following the manufacturer's protocol and incubated for 72 h at 37°C. Cells were treated with 10 μM β-secretase inhibitor IV or T-RAP and 50 μM TAT-T-RAP for 48 h in all experiments.

Alamar blue assay

To monitor the T-RAP toxicity, we performed Alamar Blue analysis (Bio-rad) following the manufacturer's instruction. After 48 h of T-RAP treatment (10 uM) or ethanol treatment in SH-SY5Y cells, the medium was substituted with a medium containing Alamar Blue. After incubating for 1 h, fluorescence in the medium was measured at 530 nm excitation and 590 nm emission wavelengths.

Preparation of membrane fractions from cells and mouse brains

Cells were washed with cold phosphate-buffered saline (PBS) then homogenized in buffer A (10 mM HEPES pH7.4, 150 mM NaCl, 10% glycerol) by Dounce homogenization using a 21G syringe at 20 strokes. After centrifugation at 1,500 g for 10 min at 4°C, the supernatant was collected. The precipitate was resuspended in buffer A and the solubilization step was repeated. The resultant supernatant was then combined with the previous one as the post-nuclear supernatant (PNS). Crude membrane fraction (MF) was obtained from PNS by ultracentrifugation at 100,000 g for 1 h at 4°C in an SW41Ti rotor (Beckman Coulter). To monitor Evectin-2 localization in membranes, MF was dissolved in RIPA buffer (50 mM Tris-HCl pH 8.0, 150 mM sodium chloride, 0.5% sodium deoxycholate, 0.1% sodium dodecyl sulfate, 1% NP-40). To analyze the lipid flippase complex formation, MF was completely dissolved in buffer A containing 1% CHAPS by a 21G syringe at 20 strokes and rotated for 1 h at 4°C. After excluding the insoluble fractions by centrifuging at 15,000 rpm for 10 min at 4°C, the supernatants were used for co-immunoprecipitation analysis. For mouse brain samples, a cerebral hemisphere was homogenized in buffer B (0.32 M sucrose, 10 mM HEPES pH 7.4, 1 mM EDTA) by Dounce homogenization at 15 strokes, then centrifuged at 1,500 g for 10 min at 4°C (step A). PNS was collected after performing the step A twice. The crude membrane isolation step of mouse brain samples was the same as described above, and then MF was dissolved in buffer C (50-mM HEPES pH 7.4, 150-mM NaCl, 1% CHAPSO). The supernatants were used for co-immunoprecipitation after centrifugation.

Co-immunoprecipitation

Cells were dissolved in IP buffer (20 mM HEPES pH 7.4, 150 mM NaCl, 0.1 mM EDTA, 1% CHAPS) for 30 min at 4°C, and total lysates were clarified by centrifuging at 15,000 rpm for 10 min at 4°C. The supernatants were rotated with the indicated antibody for 2 h at 4°C. Then, equilibrated protein G Sepharose 4 Fast Flow beads (GE Healthcare) were added and incubated overnight at 4°C. The membrane fractions from cells or mice brains were obtained using the same protocol as for total cell lysates, differing only in solubilizing buffer conditions.

GST pull-down

For GST pull-down assays, cells were lysed in 1% CHAPS lysis buffer (50 mM HEPES pH 7.4, 150 mM NaCl, 1 mM EDTA supplied with protein inhibitor cocktail [Roche]) at 4°C for 30 min. Lysates were clarified by centrifuging for 5 min at 12,000 g and incubated with GST fusion protein pre-bound to GSH-agarose beads (GE Healthcare) for 2 h at 4°C. The Laemmli sample buffer was added to each precipitate, which was subjected to immunoblotting analysis.

Iodixanol gradient fractionation

Subcellular fractionation was performed as previously described (Lee et al., 2003). Briefly, cells were homogenized in HB (250 mM Sucrose, 20 mM Tris-HCl pH 7.4, 1 mM EGTA, 1 mM EDTA) by Dounce homogenization and passing through a 21G syringe. PNS was adjusted to 25% iodixanol by mixing 50% iodixanol in HB. 50% iodixanol was prepared by 60% iodixanol solution (optiprep, Cosmo Bio). 2 mL 25% mixture was placed at the bottom of 13.2 mL ultracentrifuge tube (Beckman Coulter) and gently

overlaid with 1 mL of 20%, 18.5%, 16.5%, 14.5%, 12.5%, 10.5%, 8.5%, 6.5%, and 5% iodixanol in HB, respectively. The gradient was ultracentrifuged at 27,000 rpm (124,806 g), for 20 h at 4°C in an SW41Ti rotor. Fractions were subsequently collected from the top and TCA precipitation was performed (Trichloroacetic acid, Fujifilm-Wako). After TCA precipitation, pellets were diluted in RIPA buffer and 2× Laemmli sample buffer and analyzed by immunoblotting.

Immunoblotting

For immunoblotting analysis, aliquots of cell lysates were separated on 10% or 12% Tris-glycine gels as previously described (Kaneshiro et al., 2018). To segregate each APP-CTF and Aβ, high-resolution electrophoresis was performed using 16% Tris-Tricine gels. The separated proteins on PVDF membranes were incubated with appropriate primary antibodies overnight at 4°C and horseradish peroxidase secondary antibodies were applied for 1 h at room temperature. Membranes were detected by ImmunoStar LD or Zeta (Fujifilm-Wako), then visualized using the ChemiDoc MP Imaging System (Bio-Rad). The quantification analysis of target proteins was performed using the Image Lab software (Bio-Rad). The same protein amount was applied in all samples, and the data with no change in the loading control were processed. The densitometric intensity of each blot after subtracting the background was indicated as absolute volume and calculated percentage with controls in each experiment indicated in figure, and then processed for statistical analysis.

Immunofluorescence

Cultured cells on glass coverslips were fixed in 4% paraformaldehyde/PBS for 20 min and permeabilized with 0.1% Triton X-100/PBS for 10 min, and then washed with PBS and blocked with 1% BSA/PBS for 1 h. Coverslips were incubated with primary antibodies overnight at 4°C. After washing with 0.05% tween/PBS, coverslips were incubated with secondary antibodies for 30 min at room temperature, washed with 0.05% tween/PBS, and mounted with Vectashield with 4′,6-diamidino-2-phenylindole (Vector Laboratories, Inc). Antibodies are listed in Table S1. Stained cells were imaged on microscope BZ-X810 (Keyence) using the manufacturer's software. To increase the resolution and confirm particle focusing in Rab5-positive endosome analysis, the z-stack images were captured at 0.1 μm intervals along the z-axis using a 60×objective oil lens, and 25 z-stack images were merged into one full-focus image using BZ-X Analyzer software. Ten fields of images were randomly selected in each sample. To measure the Rab5A positive puncta size and particle distribution, all captured images were converted to binary data and automatically analyzed under the same conditions using BZ-X Analyzer Hybrid Cell Count and Macro Cell Count software (Keyence) (Salinas et al., 2020; Muko et al., 2021). The average size per particle exhibits the mean of Rab5A positive puncta area in each analyzed field of view. 30 fields (10 fields x 3 trials), 40 fields (10 fields x 4 trials), and 10 fields (10 fields x 1 trial) were quantified in Figures 1E, 6F and S2E respectively. The size distribution of Rab5A positive puncta has been shown as the percentage of the total particle counts. In 3 experiments, about 60-90 cells were analyzed. Approximately 100-300 cells per sample were analyzed in four experiments for T-RAP treatment.

Split-luciferase assay

Cells were cultured in 24-well plates (VisiPlate-24 TC 24well, PerkinElmer) and transfected proteins fused with luciferase subunits, SmBiT-Evectin-2 and LgBiT-mRab5, at 60%–70% confluence. For the effect of WT or K20E mutant on lipid flippase activity, cells were reverse transfected with plasmids and analyzed 48 h after transfection. For BACE1 inhibitor treatment, cells were reverse transfected with plasmids then treated with β-secretase inhibitor IV 24 h post-transfection. Luciferase activity was measured 48 h after treatment. For TMEM30A knockdown, luciferase activity was measured 72 h after the reverse co-transfection of shRNA-TMEM30A and luciferase subunit plasmids. For APP knockdown, cells were transfected with luciferase subunits 24 h after APP knockdown. Luciferase activity was measured 72 h after siRNA transfection. The luminescent signal was obtained by GloMax® Discover (Promega) using the Nano-Glo Live Cell Assay System (N2011, Promega) following the manufacturer's protocol. After measurement, cells were lysed with RIPA buffer, and the BCA protein assay was performed. RLU (relative light unit) except for background was set as follows. The signals obtained were normalized by protein concentration against the background sample (empty vector) to reduce transfection stress. Next, these values were normalized using the transfection ratio; the expression level of SmBiT-Evectin-2 was quantified by immunoblotting against the control sample. Background RLU indicated the obtained signal. In statistical analysis, RLU with background subtracted was applied.

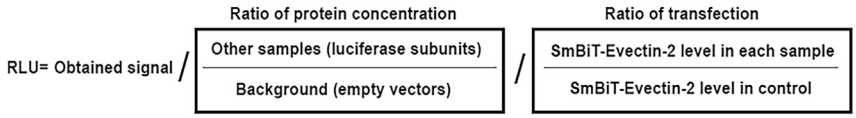

Aβ immunoprecipitation by 4G8 antibody

Aβ levels in the culture media were analyzed as previously described (Vetrivel et al., 2011). Briefly, conditioned media added 0.01% Triton X-100, 4G8 antibody, protein A/G agarose beads (Santa Cruz Biotechnologies), and then rotated overnight at 4°C. After centrifuging at 4,000 rpm for 3 min at 4°C, pellets were mixed with 4G8 wash buffer (50 mM NaCl, 10 mM Tris-HCl pH 7.6, 0.01% Triton X-100) for 20 min at 4°C. After centrifugation at 4,000 rpm, pellets mixed with 4G8 wash buffer were carefully layered on 1 mL of 1M sucrose in 4G8 wash buffer, then centrifuged at 10,000 rpm for 1 min at 4 °C. Pellets were added to 10 mM Tris-HCl pH 7.6 and gently vortexed. After centrifugation at 4,000 rpm for 3 min at 4°C, pellets were resuspended in 2× Laemmli sample buffer, and samples were boiled immediately before immunoblotting.

Preparation of synthetic Aβ oligomer

Aβ42 oligomers were prepared as previously described (Mamada et al., 2015). Briefly, human synthetic Aβ42 peptide dissolved in 1,1,1,3,3,3-hexafluoro-2-propanol (HFIP, Sigma) was evaporated then resolved in dimethyl-sulfoxide (DMSO) as 1 mg/mL stock at -20℃. Before use, Aβ42 in DMSO was sonicated in an ultrasonic bath sonicator for 10 min then diluted in DMEM/F12 phenol red-free (Fujifilm-Wako) at 100 μM and left for one day at 4℃.

QUANTIFICATION AND STATISTICAL ANALYSIS

All experimental data are expressed as the mean ± SEM. In Figures 1E, 6F and S2E, '*n*' means the number of analyzed fields of view in total trials, see also Figure legends. In other Figures, '*N*' means biological replicates, and '*n*' means the number of experiments. The experiments were analyzed with a two-tailed Student's t-test or one-way ANOVA with Bonferroni's multiple comparison test using the GraphPad Prism8 software. The statistical significance is indicated as follows: *$p < 0.05$, **$p < 0.01$, ***$p < 0.001$, and ****$p < 0.0001$.